Muon capture on deuteron and ³He

L. E. Marcucci,[1,2] M. Piarulli,[3] M. Viviani,[2] L. Girlanda,[1,2,*] A. Kievsky,[2] S. Rosati,[1,2] and R. Schiavilla[3,4]

[1]*Department of Physics, University of Pisa, IT-56127 Pisa, Italy*
[2]*INFN-Pisa, IT-56127 Pisa, Italy*
[3]*Department of Physics, Old Dominion University, Norfolk, Virginia 23529, USA*
[4]*Jefferson Lab, Newport News, Virginia 23606, USA*

The muon-capture reactions ^{2}H$(\mu^-, \nu_\mu)nn$ and ^{3}He$(\mu^-, \nu_\mu)^3$H are studied with conventional or chiral realistic potentials and consistent weak currents. The initial and final $A = 2$ and $A = 3$ nuclear wave functions are obtained from the Argonne v_{18} or chiral next-to-next-to-next-to leading order (N3LO) two-nucleon potential, in combination with, respectively, the Urbana IX or chiral next-to-next-to leading order (N2LO) three-nucleon potential in the case of $A = 3$. The weak current consists of polar- and axial-vector components. The former are related to the isovector piece of the electromagnetic current via the conserved-vector-current hypothesis. These and the axial currents are derived either in a meson-exchange or in a chiral effective field theory (χEFT) framework. There is one parameter (either the N-to-Δ axial coupling constant in the meson-exchange model, or the strength of a contact term in the χEFT model) that is fixed by reproducing the Gamow-Teller matrix element in tritium β decay. The model dependence relative to the adopted interactions and currents (and cutoff sensitivity in the χEFT currents) is weak, resulting in total rates of 392.0 ± 2.3 s^{-1} for $A = 2$, and 1484 ± 13 s^{-1} for $A = 3$, where the spread accounts for this model dependence.

I. INTRODUCTION

There is a significant body of experimental and theoretical work on muon capture in nuclei (see Refs. [1,2] for a review). These processes provide a testing ground for wave functions and, indirectly, the interactions from which these are obtained, and for models of the nuclear weak current. This is particularly important for neutrino reactions in light nuclei [3] and for processes, such as the astrophysically relevant weak captures on proton and ³He, the rates of which can not be measured experimentally, and for which one has to rely exclusively on theory. Thus, it becomes crucial to study within the same theoretical framework related electroweak transitions, for which the rates are known experimentally [4]. Muon captures are among such reactions.

In this paper, we focus our attention on muon capture on deuteron and ³He, i.e., on the reactions

$$\mu^- + d \rightarrow n + n + \nu_\mu, \qquad (1.1)$$

$$\mu^- + {}^3\text{He} \rightarrow {}^3\text{H} + \nu_\mu. \qquad (1.2)$$

Muon capture on ³He can also occur through the two- (nd) and three-body (nnp) breakup channels of ³H. However, the branching ratios of these two processes are 20% and 10%, respectively, and will not be considered in this paper.

These reactions have been studied extensively, both experimentally and theoretically, through the years. In reaction (1.1), the stopped muons are captured from two hyperfine states $f = 1/2$ or $3/2$. The doublet capture rate Γ^D has been calculated by several groups to be about 40 times larger than the quadruplet [1,2]. We will therefore consider only Γ^D. The

first attempt to measure Γ^D was carried out over 40 years ago by Wang *et al.*: they obtained $\Gamma^D = 365(96)$ s^{-1} [5]. A few years later, Bertin *et al.* measured $\Gamma^D = 445(60)$ s^{-1} [6]. Measurements performed in the 1980s gave $\Gamma^D = 470(29)$ s^{-1} [7] and $\Gamma^D = 409(40)$ s^{-1} [8]. These measurements, while consistent with each other, are not very precise: the errors are in the 6% –10% range. However, there is hope to have this situation clarified by the MuSun Collaboration [9], which is expected to perform an experiment at the Paul Scherrer Institut, with the goal of measuring Γ^D with a precision of 1%.

The experimental situation for reaction (1.2) is much clearer: after a first set of measurements in the early 1960s [10–13], a very precise determination in the late 1990s yielded a total capture rate $\Gamma_0 = 1496(4)$ s^{-1} [14], a value consistent with those of the earlier measurements, although these were affected by considerably larger uncertainties.

Theoretical work on reactions (1.1) and (1.2) is just as extensive, and a list of publications, updated to the late 1990s, is given in Table 4.1 of Ref. [1], and in Ref. [2]. Here, we limit our considerations to the calculations of Refs. [15–17]. We also comment on the recent studies of Ando *et al.* [18] and Ricci *et al.* [19].

The calculations of Refs. [15–17] were performed within the standard nuclear physics approach (SNPA): their authors used the realistic potential models available at the time to obtain the nuclear wave functions, and included in the nuclear weak current operator one- (impulse approximation) and two-body operators. In Ref. [15], Γ^D was calculated to be 416(7) s^{-1}, with the uncertainty coming from imprecise knowledge of the coupling constants, and, in Refs. [16] and [17], 399 and 402 s^{-1}, respectively. The results of Refs. [16] and [17] are in good agreement with each other, while that of Ref. [15] differs by ∼4%. It is important to note, however, that the meson-exchange-currents (MEC) contributions were not

---

*Current address: Department of Physics, University of Salento, and INFN-Lecce, IT-73100 Lecce, Italy.

constrained to reproduce any experimental observable, such as the triton half-life, as is now common practice [20–22].

Reference [18] overcame some of the limitations inherent in the earlier studies. Much along the lines of Ref. [22], reaction (1.1) was studied within a hybrid chiral effective field theory (χEFT) approach, in which matrix elements of weak operators derived in χEFT were evaluated between wave functions obtained from a realistic potential, specifically the Argonne v_{18} (AV18) [23]. The χEFT axial current contains a low-energy constant, which was fixed by reproducing the experimental Gamow-Teller matrix element (GT^{EXP}) in tritium β decay. The calculation, however, retained only the S-wave contribution in the nn final scattering state (the $^1S_0$ state), and higher partial-wave contributions were taken from Ref. [16]. This approach yielded a value for Γ^D of 386 s^{-1}, with $\Gamma^D(^1S_0) = 245(1)$ s^{-1}, the theoretical error being related to the experimental uncertainty in GT^{EXP}.

The latest SNPA calculation of muon capture on deuteron has been carried out in Ref. [19], and has led to values in the range of 416–430 s^{-1} (see Table 1 of Ref. [19]), depending on the potential used, i.e., the Nijmegen I or Nijmegen 93 [24]. However, the model for the axial current is not constrained by data, resulting in the relatively large spread in Γ^D values.

Finally, there is a calculation based on pionless EFT [25] with the objective of constraining the two-nucleon axial-current matrix element by reproducing the muon-capture rate on deuterons. This same matrix element enters the pp weak capture.

Theoretical studies for reaction (1.2) within the SNPA have been performed in the early 1990s by Congleton and Fearing [26] and Congleton and Truhlik [27]. In the later work, the nuclear wave functions were obtained from a realistic Hamiltonian based on the Argonne v_{14} (AV14) two-nucleon [28] and the Tucson-Melbourne (TM) three-nucleon [29] interactions. The nuclear weak current retained contributions similar to those of Ref. [19]. The value obtained for the total capture rate Γ_0 was 1502(32) s^{-1}, with the uncertainty due to poor knowledge of some of the coupling constants and cutoff parameters entering the axial current.

A first study of the model dependence of predictions for the total rate of muon capture on ^{3}He was carried out in Ref. [30], within the SNPA, but without the inclusion of MEC contributions. Values for Γ_0 were found to vary by $\simeq 100$ s^{-1}, depending on the potential model considered. Both old- (Paris [31], Bonn A and B [32], AV14) and new-generation (Nijmegen I [24] and CD-Bonn [33]) potentials were used. However, no three-nucleon forces were included. This second aspect of the calculation, along with the absence of MEC contributions, might be the origin of the large model dependence observed in the results.

A first attempt to study muon capture on ^{3}He in a way that was consistent with the approach adopted for the weak proton-capture reactions involved some of the present authors [34]. The nuclear wave functions were obtained with the hyperspherical-harmonics (HH) method (see Ref. [35] for a recent review) from a realistic Hamiltonian based on the AV18 two-nucleon and Urbana IX [36] (UIX) three-nucleon interactions. The model for the nuclear weak current was taken from Refs. [20,21]. However, two additional contributions were

included: the single-nucleon pseudoscalar charge operator and the pseudoscalar two-body term in the N-to-Δ transition axial current. Both contributions are of order $O(q^2/m^2)$, where q is the momentum transfer in the process and m is the nucleon mass, and were obviously neglected in the pp and hep captures of Refs. [20,21], for which $q \ll m$. The axial coupling constant for the N-to-Δ transition was constrained to reproduce GT^{EXP}. The total capture rate Γ_0 was found to be 1484(8) s^{-1}, where the uncertainty results from the adopted fitting procedure and experimental error on GT^{EXP}. A calculation based on the older AV14-TM Hamiltonian model yielded a Γ_0 of 1486(8) s^{-1}, suggesting a weak model dependence.

Recently, a hybrid calculation has appeared [37] in which the nuclear wave functions have been obtained with the effective interaction HH method [38], and the χEFT weak current is that of Ref. [22]. It has yielded a value for Γ_0 of 1499(16) s^{-1}, where the error has two main sources: the experimental uncertainty on the triton half-life and the calculation of radiative corrections.

In light of the previous considerations, it is clear that still lacking is a calculation that (i) treats reactions (1.1) and (1.2) simultaneously in a consistent framework, either SNPA or χEFT; (ii) is based on up-to-date Hamiltonian models to generate the wave functions; and (iii) reduces the model dependence of the weak axial current by constraining it to reproduce GT^{EXP}. The goal of this paper is to fill this gap. The calculation has been structured as follows. The nuclear Hamiltonian models considered consist of the AV18 and next-to-next-to-next-to leading order (N3LO) [39] two-nucleon interactions for the $A = 2$ systems, augmented by the UIX and next-to-next-to leading order (N2LO) [40] three-nucleon interactions for the $A = 3$ systems. The nuclear weak current is derived from either SNPA or χEFT. In both cases, its axial component is calibrated by fitting GT^{EXP}, while its vector part is related to the isovector electromagnetic current by the conserved-vector-current (CVC) hypothesis. The SNPA version of it reproduces well the static magnetic properties of few-nucleon systems. In the χEFT electromagnetic current of Ref. [41], adopted in this paper, the two low-energy constants are fixed by reproducing the trinucleon magnetic moments.

In closing, we note that the study of Ref. [34] has established that the total rate of reaction (1.2) scales approximately linearly with the trinucleon binding energy. Thus, a realistic calculation of this rate must, at a minimum, include a three-nucleon potential that can well reproduce these energies (as is the case here). Finally, we could have adopted the set of two-nucleon chiral potentials at N3LO derived by the Bonn group [42] for a range of cutoff parameters Λ in order to explore the sensitivity of the results to the short-range behavior of the potentials. However, the potentials considered in this study (AV18 and N3LO) have such drastically different treatments of this short-range behavior that they should provide a meaningful measure of the model dependence originating from it.

The paper is organized as follows. In Sec. II, we list the explicit expressions for the observables of interest in terms of reduced matrix elements of multipole operators. In the case of reaction (1.2), the derivation is given in Ref. [34]. In Sec. III, we briefly review the method used to calculate the nuclear wave functions and summarize the main results for the observables

of the nuclear systems involved in the reactions of interest. In Sec. IV, we describe the model for the nuclear weak current, both its SNPA and χEFT versions. In Sec. V, we present and discuss the results obtained for the total capture rates of reactions (1.1) and (1.2), and, finally, in Sec. VI we summarize our conclusions.

II. OBSERVABLES

The muon capture on deuteron and ^{3}He is induced by the weak interaction Hamiltonian [43]

$$H_W = \frac{G_V}{\sqrt{2}} \int d\mathbf{x}\, l_\sigma(\mathbf{x}) j^\sigma(\mathbf{x}) , \quad (2.1)$$

where G_V is the Fermi coupling constant, $G_V = 1.149\,39 \times 10^{-5}$ GeV^{-2} as obtained from an analysis of 0^+ to 0^+ β decays [44], and l_σ and j^σ are the leptonic and hadronic current densities, respectively. The former is given by

$$l_\sigma(\mathbf{x}) = e^{-i\mathbf{k}_\nu \cdot \mathbf{x}} \overline{u}(\mathbf{k}_\nu, h_\nu) \gamma_\sigma (1 - \gamma_5) \psi_\mu(\mathbf{x}, s_\mu), \quad (2.2)$$

where $\psi_\mu(\mathbf{x}, s_\mu)$ is the ground-state wave function of the muon in the Coulomb field of the nucleus in the initial state, and $u(\mathbf{k}_\nu, h_\nu)$ is the spinor of a muon neutrino with momentum $\mathbf{k}_\nu$, energy E_ν ($=k_\nu$), and helicity h_ν. While, in principle, the relativistic solution of the Dirac equation could be used, in practice it suffices to approximate

$$\psi_\mu(\mathbf{x}, s_\mu) \simeq \psi_{1s}(x)\chi(s_\mu) \equiv \psi_{1s}(x)u(\mathbf{k}_\mu, s_\mu)$$
$$\mathbf{k}_\mu \to 0, \quad (2.3)$$

since the muon velocity $v_\mu \simeq Z\alpha \ll 1$ (α is the fine-structure constant and $Z = 1$ or $Z = 2$ for deuteron or ^{3}He, respectively). Here, $\psi_{1s}(x)$ is the $1s$ solution of the Schrödinger equation and, since the muon is essentially at rest, it is justified to replace the two-component spin state $\chi(s_\mu)$ with the four-component spinor $u(\mathbf{k}_\mu, s_\mu)$ in the limit $\mathbf{k}_\mu \to 0$. This will allow us to use standard techniques to carry out the spin sum over s_μ at a later stage.

In order to account for the hyperfine structure in the initial system, the muon and deuteron or ^{3}He spins are coupled to states with total spin f, equal to $1/2$ or $3/2$ in the deuteron case, and to 0 or 1 in the ^{3}He case. The transition amplitude can then be conveniently written as

$$T_W(f, f_z; s_1, s_2, h_\nu) \equiv \langle nn, s_1, s_2; \nu, h_\nu | H_W | (\mu, d); f, f_z \rangle$$
$$\simeq \frac{G_V}{\sqrt{2}} \psi_{1s}^{av} \sum_{s_\mu s_d} \left\langle \frac{1}{2} s_\mu, 1 s_d \middle| f f_z \right\rangle$$
$$\times l_\sigma(h_\nu, s_\mu) \langle \Psi_{\mathbf{p}, s_1 s_2}(nn) | j^\sigma(\mathbf{q}) | \Psi_d(s_d) \rangle, \quad (2.4)$$

for the muon capture on deuteron, where $\mathbf{p}$ is the nn relative momentum, and [34]

$$T_W(f, f_z; s_3', h_\nu) \equiv \langle {}^3\text{H}, s_3'; \nu, h_\nu | H_W | (\mu, {}^3\text{He}); f, f_z \rangle$$
$$\simeq \frac{G_V}{\sqrt{2}} \psi_{1s}^{av} \sum_{s_\mu s_3} \left\langle \frac{1}{2} s_\mu, \frac{1}{2} s_3 \middle| f f_z \right\rangle$$
$$\times l_\sigma(h_\nu, s_\mu) \langle \Psi_{{}^3\text{H}}(s_3') | j^\sigma(\mathbf{q}) | \Psi_{{}^3\text{He}}(s_3) \rangle, \quad (2.5)$$

for muon capture on ^{3}He. In Eqs. (2.4) and (2.5) we have defined

$$l_\sigma(h_\nu,\, s_\mu) \equiv \overline{u}(\mathbf{k}_\nu, h_\nu)\, \gamma_\sigma\, (1 - \gamma_5)u(\mathbf{k}_\mu, s_\mu), \quad (2.6)$$

and the Fourier transform of the nuclear weak current has been introduced as

$$j^\sigma(\mathbf{q}) = \int d\mathbf{x}\, e^{i\mathbf{q}\cdot\mathbf{x}}\, j^\sigma(\mathbf{x}) \equiv (\rho(\mathbf{q}), \mathbf{j}(\mathbf{q})), \quad (2.7)$$

with the leptonic momentum transfer $\mathbf{q}$ defined as $\mathbf{q} = \mathbf{k}_\mu - \mathbf{k}_\nu \simeq -\mathbf{k}_\nu$. The function $\psi_{1s}(x)$ has been factored out from the matrix element of $j^\sigma(\mathbf{q})$ between the initial and final states. For muon capture on deuteron, ψ_{1s}^{av} is approximated as [43]

$$\left| \psi_{1s}^{av} \right|^2 \equiv |\psi_{1s}(0)|^2 = \frac{(\alpha\,\mu_{\mu d})^3}{\pi}, \quad (2.8)$$

where $\psi_{1s}(0)$ denotes the Bohr wave function for a point charge e evaluated at the origin, and $\mu_{\mu d}$ is the reduced mass of the (μ, d) system. For muon capture on ^{3}He, ψ_{1s}^{av} is approximated as [34]

$$\left| \psi_{1s}^{av} \right|^2 \equiv \mathcal{R}\, \frac{(2\,\alpha\,\mu_{\mu^3\text{He}})^3}{\pi}, \quad (2.9)$$

where, in this case, $\mu_{\mu^3\text{He}}$ is the reduced mass of the $(\mu, {}^3\text{He})$ system, and the factor $\mathcal{R}$ approximately accounts for the finite extent of the nuclear charge distribution [43]. This factor is defined as

$$\mathcal{R} = \frac{\left| \psi_{1s}^{av} \right|^2}{|\psi_{1s}(0)|^2}, \quad (2.10)$$

with

$$\psi_{1s}^{av} = \frac{\int d\mathbf{x}\, e^{i\mathbf{q}\cdot\mathbf{x}}\psi_{1s}(x)\rho(x)}{\int d\mathbf{x}\, e^{i\mathbf{q}\cdot\mathbf{x}}\rho(x)}, \quad (2.11)$$

where $\rho(x)$ is the ^{3}He charge density. It has been calculated explicitly by using the charge densities corresponding to the two Hamiltonian models considered in this study (AV18/UIX and N3LO/N2LO), and has been found to be, for both models, within a percent of 0.98, the value obtained from the experimental charge density and commonly adopted in the literature [43].

In the case of muon capture on deuteron, the final-state wave function is expanded in partial waves as

$$\Psi_{\mathbf{p}, s_1, s_2}(nn) = 4\pi \sum_S \left\langle \frac{1}{2} s_1, \frac{1}{2} s_2 \middle| S S_z \right\rangle$$
$$\times \sum_{LJJ_z} i^L Y_{LL_z}^*(\hat{\mathbf{p}}) \langle S S_z, L L_Z | J J_z \rangle\, \overline{\Psi}_{nn}^{LSJJ_z}(p), \quad (2.12)$$

where $\overline{\Psi}_{nn}^{LSJJ_z}(p)$ is the nn wave function, and will be discussed in Sec. III. In this paper, we restrict our calculation to $J \leqslant 2$ and $L \leqslant 3$ and, therefore, the contributing partial waves are, in a spectroscopic notation, $^1S_0$, $^3P_0$, $^3P_1$, $^3P_2$–$^3F_2$, and $^1D_2$.

Standard techniques [21,43] are now used to carry out the multipole expansion of the weak charge $\rho(\mathbf{q})$ and current $\mathbf{j}(\mathbf{q})$

operators. For muon capture on deuteron, we find

$$\left\langle \overline{\Psi}_{nn}^{LSJJ_z}(p) \middle| \rho(\mathbf{q}) \middle| \Psi_d(s_d) \right\rangle$$
$$= \sqrt{4\pi} \sum_{\Lambda \geqslant 0} \sqrt{2\Lambda + 1} \, i^{\Lambda} \frac{\langle 1s_d, \Lambda 0 | J J_z \rangle}{\sqrt{2J+1}} C_{\Lambda}^{LSJ}(q) , \tag{2.13}$$

$$\left\langle \overline{\Psi}_{nn}^{LSJJ_z}(p) \middle| j_z(\mathbf{q}) \middle| \Psi_d(s_d) \right\rangle$$
$$= -\sqrt{4\pi} \sum_{\Lambda \geqslant 0} \sqrt{2\Lambda + 1} \, i^{\Lambda} \frac{\langle 1s_d, \Lambda 0 | J J_z \rangle}{\sqrt{2J+1}} L_{\Lambda}^{LSJ}(q) , \tag{2.14}$$

$$\left\langle \overline{\Psi}_{nn}^{LSJJ_z}(p) \middle| j_\lambda(\mathbf{q}) \middle| \Psi_d(s_d) \right\rangle$$
$$= \sqrt{2\pi} \sum_{\Lambda \geqslant 1} \sqrt{2\Lambda + 1} \, i^{\Lambda} \frac{\langle 1s_d, \Lambda - \lambda | J J_z \rangle}{\sqrt{2J+1}}$$
$$\times \left[-\lambda M_{\lambda}^{LSJ}(q) + E_{\Lambda}^{LSJ}(q) \right] , \tag{2.15}$$

where $\lambda = \pm 1$, and $C_{\Lambda}^{LSJ}(q)$, $L_{\Lambda}^{LSJ}(q)$, $E_{\Lambda}^{LSJ}(q)$, and $M_{\Lambda}^{LSJ}(q)$ denote the reduced matrix elements (RMEs) of the Coulomb (C), longitudinal (L), and transverse-electric (E) and transverse-magnetic (M) multipole operators, as defined in Ref. [21]. Since the weak charge and current operators have scalar/polar-vector (V) and pseudoscalar/axial-vector (A) components, each multipole consists of the sum of V and A terms, having opposite parity under space inversions [21]. The contributing multipoles for the S, P, and D channels considered in this paper are listed in Table I, where the superscripts LSJ have been dropped.

In the case of muon capture on ^{3}He, explicit expressions for the multipole operators can be found in Ref. [34]. Here, we only note that parity and angular-momentum selection rules restrict the contributing RMEs to $C_0(V)$, $C_1(A)$, $L_0(V)$, $L_1(A)$, $E_1(A)$, and $M_1(V)$.

The total capture rate for the two reactions under consideration is then defined as

$$d\Gamma = 2\pi \delta(\Delta E) \overline{|T_W|^2} \times (\text{phase space}), \tag{2.16}$$

TABLE I. Contributing multipoles in muon capture on deuteron for all the *nn* partial waves with $J \leqslant 2$ and $L \leqslant 3$. The spectroscopic notation is used. See text for further explanations.

Partial wave	Contributing multipoles
$^1S_0$	$C_1(A), L_1(A), E_1(A), M_1(V)$
$^3P_0$	$C_1(V), L_1(V), E_1(V), M_1(A)$
$^3P_1$	$C_0(A), L_0(A),$ $C_1(V), L_1(V), E_1(V), M_1(A),$ $C_2(A), L_2(A), E_2(A), M_2(V)$
$^3P_2$–$^3F_2$	$C_1(V), L_1(V), E_1(V), M_1(A),$ $C_2(A), L_2(A), E_2(A), M_2(V),$ $C_3(V), L_3(V), E_3(V), M_3(A)$
$^1D_2$	$C_1(A), L_1(A), E_1(A), M_1(V),$ $C_2(V), L_2(V), E_2(V), M_2(A),$ $C_3(A), L_3(A), E_3(A), M_3(V)$

where $\delta(\Delta E)$ is the energy-conserving δ function, and the phase space is $d\mathbf{p}\,d\mathbf{k}_\nu/(2\pi)^6$ for reaction (1.1) and just $d\mathbf{k}_\nu/(2\pi)^3$ for reaction (1.2). The following notation has been introduced: (i) for muon capture on deuteron,

$$\overline{|T_W|^2} = \frac{1}{2f+1} \sum_{s_1 s_2 h_\nu} \sum_{f_z} |T_W(f, f_z; s_1, s_2, h_\nu)|^2, \tag{2.17}$$

and the initial hyperfine state has been fixed to be $f = 1/2$; (ii) for muon capture on ^{3}He,

$$\overline{|T_W|^2} = \frac{1}{4} \sum_{s_3' h_\nu} \sum_{f f_z} |T_W(f, f_z; s_3', h_\nu)|^2, \tag{2.18}$$

and the factor 1/4 follows from assigning the same probability to the different hyperfine states.

After carrying out the spin sums, the total rate for muon capture on ^{3}He reads [34] as

$$\Gamma_0 = G_V^2 \, E_\nu^2 \left(1 - \frac{E_\nu}{m_{^3\text{H}}} \right) |\psi_{1s}^{\text{av}}|^2 \big[|C_0(V) - L_0(V)|^2$$
$$+ |C_1(A) - L_1(A)|^2 + |M_1(V) - E_1(A)|^2 \big], \tag{2.19}$$

with E_ν given by

$$E_\nu = \frac{(m_\mu + m_{^3\text{He}})^2 - m_{^3\text{H}}^2}{2(m_\mu + m_{^3\text{He}})}. \tag{2.20}$$

In the case of muon capture on deuteron, the differential rate reads

$$\frac{d\Gamma_D}{dp} = E_\nu^2 \left[1 - \frac{E_\nu}{(m_\mu + m_d)} \right] |\psi_{1s}^{\text{av}}|^2 \frac{p^2 d\hat{\mathbf{p}}}{8\pi^4} \overline{|T_W|^2}, \tag{2.21}$$

where

$$E_\nu = \frac{(m_\mu + m_d)^2 - 4m_n^2 - 4p^2}{2(m_\mu + m_d)}. \tag{2.22}$$

In Eqs. (2.19)–(2.22), m_μ, m_n, m_d, $m_{^3\text{H}}$, and $m_{^3\text{He}}$ are the muon, neutron, deuteron, ^{3}H, and ^{3}He masses, respectively. The integration over $\hat{\mathbf{p}}$ in Eq. (2.21) is performed numerically using Gauss-Legendre points, and a limited number of them, of the order of 10, are necessary to achieve convergence to better than 1 part in 10^3. In order to calculate the total capture rate Γ^D, the differential capture rate is plotted versus p and numerically integrated. Usually, about 30 points in p are enough for this integration in each partial wave. The differential cross section for each contributing partial wave will be shown in Sec. V.

III. NUCLEAR WAVE FUNCTIONS

Bound and continuum wave functions for both two- and three-nucleon systems are obtained with the hyperspherical-harmonics (HH) expansion method. This method, as implemented in the case of $A = 3$ systems, has been reviewed in considerable detail in a series of recent publications [35,45,46]. We will discuss it here in the context of $A = 2$ systems, for which, of course, wave functions could have been obtained by direct solution of the Schrödinger equation.

The nuclear wave function for a bound system of total angular momentum JJ_z can generally be written as

$$|\Psi^{JJ_z}\rangle = \sum_\mu c_\mu |\Psi_\mu^{JJ_z}\rangle, \qquad (3.1)$$

where $|\Psi_\mu^{JJ_z}\rangle$ is a complete set of states, and μ is an index denoting the set of quantum numbers necessary to completely specify the basis elements. The coefficients of the expansion can be calculated by using the Rayleigh-Ritz variational principle, which states that

$$\langle \delta_c \Psi^{JJ_z} | H - E | \Psi^{JJ_z} \rangle = 0, \qquad (3.2)$$

where $\delta_c \Psi^{JJ_z}$ indicates the variation of Ψ^{JJ_z} for arbitrary infinitesimal changes of the linear coefficients c_μ. The problem of determining c_μ and the energy E is then reduced to a generalized eigenvalue problem

$$\sum_{\mu'} \langle \Psi_\mu^{JJ_z} | H - E | \Psi_{\mu'}^{JJ_z} \rangle c_{\mu'} = 0. \qquad (3.3)$$

In the case of the deuteron, we first define

$$\psi_{LSJJ_z}(\mathbf{r}) = F_{LSJ}(r) \mathcal{Y}_{LSJJ_z}(\hat{\mathbf{r}}), \qquad (3.4)$$

where

$$\mathcal{Y}_{LSJJ_z}(\hat{\mathbf{r}}) = [Y_L(\hat{\mathbf{r}}) \otimes \chi_S]_{JJ_z}, \qquad (3.5)$$

and $\mathbf{r}$ is the relative position vector of the two nucleons. Obviously, for the deuteron, $L = 0$ or 2, $S = 1$, $J = 1$, and $T = 0$ (the isospin state η_{TT_z} with $T = T_z = 0$ has been dropped for brevity). The radial functions $F_{LSJ}(r)$ are then conveniently expanded on a basis of Laguerre polynomials as

$$F_{LSJ}(r) = \sum_l c_{LSJ,l} f_l(r), \qquad (3.6)$$

with

$$f_l(r) = \sqrt{\frac{l!}{(l+2)!}} \gamma^{3/2} L_l^{(2)}(\gamma r) e^{-\gamma r/2}, \qquad (3.7)$$

where the parameter γ is variationally optimized (γ is in the range of 3–4 fm^{-1} for the AV18 and N3LO potentials). The complete wave function is then reconstructed as

$$\Psi^{1J_z} = \sum_{L=0,2} \sum_l c_{L11,l} f_l(r) \mathcal{Y}_{L11J_z}(\hat{\mathbf{r}})$$
$$\equiv \sum_\mu c_\mu \Psi_\mu^{1J_z}, \qquad (3.8)$$

and the subscript μ denotes the set of quantum numbers $[L, S = 1, J = 1, l]$.

The nn continuum wave function is written as

$$\Psi^{LSJJ_z} = \Psi_C^{LSJJ_z} + \Psi_A^{LSJJ_z}, \qquad (3.9)$$

where $\Psi_C^{LSJJ_z}$ describes the system in the region where the two neutrons are close to each other and their mutual interactions are strong, while $\Psi_A^{LSJJ_z}$ describes their relative motion in the asymptotic region. The function $\Psi_C^{LSJJ_z}$, which vanishes in the limit of large separations, is expanded on Laguerre polynomials as before for the case of the deuteron

[see Eq. (3.1)], while the function $\Psi_A^{LSJJ_z}$ is the appropriate asymptotic solution in channel LSJ:

$$\Psi_A^{LSJJ_z} = \sum_{L'S'} \left[\delta_{LL'} \delta_{SS'} \Omega_{L'S'JJ_z}^R + \mathcal{R}_{LS,L'S'}^J(p) \Omega_{L'S'JJ_z}^I \right], \qquad (3.10)$$

where

$$\Omega_{LSJJ_z}^{R/I} = R_L^{R/I}(pr) \mathcal{Y}_{LSJJ_z}(\hat{\mathbf{r}}), \qquad (3.11)$$

with

$$R_L^R(pr) \equiv \frac{1}{p^L} j_L(pr),$$
$$R_L^I(pr) \equiv p^{L+1} f_R(r) n_L(pr), \qquad (3.12)$$

with p being the magnitude of the relative momentum. The functions $j_L(pr)$ and $n_L(pr)$ are the regular and irregular spherical Bessel functions, and $f_R(r) = [1 - \exp(-br)]^{2L+1}$ has been introduced to regularize $n_L(pr)$ at small values of r. The trial parameter b is taken as $b = 0.25$ fm^{-1}.

The matrix elements $\mathcal{R}_{LS,L'S'}^J(p)$ and the coefficients c_μ entering the expansion of $\Psi_C^{LSJJ_z}$ are determined applying the Kohn variational principle [47], stating that the functional

$$\left[\mathcal{R}_{LS,L'S'}^J(p) \right]$$
$$= \mathcal{R}_{LS,L'S'}^J(p) - \frac{2\mu_{nn}}{\hbar^2} \langle \Psi^{L'S'JJ_z} | H - \frac{p^2}{2\mu_{nn}} | \Psi^{LSJJ_z} \rangle, \qquad (3.13)$$

is stationary with respect to variations of the trial parameters in Ψ^{LSJJ_z}. Here, μ_{nn} is the reduced mass of the nn system. Performing the variation, a system of linear inhomogeneous equations for c_μ and a set of algebraic equations for $\mathcal{R}_{LS,L'S'}^J(p)$ are derived and solved by standard techniques. From the $\mathcal{R}_{LS,L'S'}^J(p)$, phase shifts, mixing angles, and scattering lengths are easily obtained.

We list in Tables II and III the binding energies and scattering lengths calculated with the Hamiltonian models considered in this work. Note that the $A = 3$ wave functions retain both $T = 1/2$ and $T = 3/2$ contributions, with T being the total isospin quantum number. The experimental data are, in general, quite well reproduced. It should be noted that, by using only two-nucleon interaction, the triton and ³He binding energies are 7.624 and 6.925 MeV with the AV18, and 7.854 and 7.128 MeV with the N3LO, respectively.

TABLE II. Deuteron binding energy B_d (in MeV) and D-state probability (in %), nn and singlet and triplet np scattering lengths (in fm), calculated with the two-nucleon potentials AV18 and N3LO. The experimental results are from Ref. [39].

	AV18	N3LO	Experiment
B_d (MeV)	2.22457	2.22456	2.224574(9)
P_D (%)	5.76	4.51	
a_{nn} (fm)	−18.487	−18.900	−18.9(4)
$^1a_{np}$ (fm)	−23.732	−23.732	−23.740(20)
$^3a_{np}$ (fm)	5.412	5.417	5.419(7)

TABLE III. Triton and ^{3}He binding energies $B_{^3\mathrm{H}}$ and $B_{^3\mathrm{He}}$ (in MeV), and nd doublet and quartet scattering lengths (in fm), calculated with the two- and three-nucleon potentials AV18/UIX and N3LO/N2LO. The experimental results are from Ref. [35].

	AV18/UIX	N3LO/N2LO	Experiment
$B_{^3\mathrm{H}}$ (MeV)	8.479	8.474	8.482
$B_{^3\mathrm{He}}$ (MeV)	7.750	7.733	7.718
$^2a_{nd}$ (fm)	0.590	0.675	0.645(3)(7)
$^4a_{nd}$ (fm)	6.343	6.342	6.35(2)

Finally, we define

$$\overline{\Psi}^{LSJJ_z} = \sum_{L'S'} \left[\delta_{LL'}\delta_{SS'} - i\,\mathcal{R}^J_{LS,L'S'}(p) \right]^{-1} \Psi^{L'S'JJ_z}, \quad (3.14)$$

so that $\overline{\Psi}^{LSJJ_z}$ has unit flux. The function $\overline{\Psi}^{LSJJ_z}$ enters in Eq. (2.12) and in the expression for differential muon capture rate on deuteron.

IV. WEAK TRANSITION OPERATOR

The nuclear weak charge and current operators consist of polar- and axial-vector components. In this paper, we consider two different models, both of which have been used in studies of weak pp and hep capture reactions in the energy regime relevant to astrophysics [20–22]. The first model has been developed within the so-called "Standard Nuclear Physics Approach" (SNPA) and has been applied also to study weak transitions for $A = 6$ and $A = 7$ nuclei [48], and magnetic moments and $M1$ widths of nuclei with $A \leqslant 7$ [49,50]. It will be discussed in Sec. IV A. In the second model, the nuclear weak transition operators have been derived in heavy-baryon chiral perturbation theory (HBChPT), carrying out the expansion up to next-to-next-to-next-to leading order (N3LO) [22,51]. This same model has been updated and most recently used in the electromagnetic sector to study the three-nucleon magnetic moments and np and nd radiative capture reactions in Ref. [41]. We review it in Sec. IV B.

A. The "Standard Nuclear Physics Approach"

The one-body axial charge and current operators have the standard expressions [21] obtained from the nonrelativistic reduction of the covariant single-nucleon current, and include terms proportional to $1/m^2$, with m being the nucleon mass. The induced-pseudoscalar contributions are retained both in the axial current and charge operators, and are given by

$$\rho^{(1)}_{i,PS}(\mathbf{q}; A) = -\frac{g_{PS}(q_\sigma^2)}{2\,m\,m_\mu} \tau_{i,-}(m_\mu - E_\nu)(\boldsymbol{\sigma}_i \cdot \mathbf{q})\, e^{i\mathbf{q}\cdot\mathbf{r}_i}, \quad (4.1)$$

$$\mathbf{j}^{(1)}_{i,PS}(\mathbf{q}; A) = -\frac{g_{PS}(q_\sigma^2)}{2\,m\,m_\mu} \tau_{i,-}\,\mathbf{q}\,(\boldsymbol{\sigma}_i \cdot \mathbf{q})\, e^{i\mathbf{q}\cdot\mathbf{r}_i}, \quad (4.2)$$

where

$$\tau_{i,-} = (\tau_{i,x} - i\tau_{i,y})/2\,, \quad (4.3)$$

and $\mathbf{q}$ is the three-momentum transfer, m_μ is the muon mass, E_ν is the neutrino energy, and q_σ^2 is the squared four-momentum

transfer. Note that, since in the present case $\mathbf{q}$ is not negligible ($q \simeq m_\mu$), axial and induced-pseudoscalar form factors need be included. In the notation of Ref. [34], they are taken as

$$g_A(q_\sigma^2) = \frac{g_A}{\left(1 + q_\sigma^2/\Lambda_A^2\right)^2}, \quad (4.4)$$

$$g_{PS}(q_\sigma^2) = -\frac{2\,m_\mu\,m}{m_\pi^2 + q_\sigma^2}\,g_A(q_\sigma^2). \quad (4.5)$$

For the axial-vector coupling constant g_A, two values have been adopted in this study: the first one, $g_A = 1.2654(42)$, is taken from Ref. [52], and has been used widely in studies of weak processes [21,22,34,48]. The second one, $g_A = 1.2695(29)$, is the latest determination quoted by the Particle Data Group (PDG) [53]. The two values for g_A are consistent with each other. To compare with the results of the aforementioned studies, we have adopted the earlier determination for g_A. On the other hand, to estimate the theoretical uncertainty arising from this source, the calculation has been carried out also using $g_A = 1.2695(29)$ in one specific case. As it will be shown in the following, the central value and the theoretical uncertainties of the considered observables are comparable in both cases.

The value for the cutoff mass Λ_A used in this work is 1 GeVc^2, as in Ref. [34]. It is obtained from an analysis of pion electroproduction data [54] and measurements of the reaction $\nu_\mu + p \to n + \mu^+$ [55]. Uncertainties in the q_σ^2 dependence of the axial form factor, in particular the value of Λ_A, could significantly impact predictions for the muon rates under consideration, although the present level of agreement achieved between theory and experiment (see Sec. V) suggests that this uncertainty in Λ_A is at the few percent level. This is at variance with current analyses of neutrino quasielastic scattering data on nuclear targets [56], which obtain Λ_A values in the range 1.20–1.35 GeVc^2. However, it is important to emphasize that these analyses are based on rather crude models of nuclear structure (Fermi gas or local density approximations of the nuclear matter spectral function) as well as on simplistic treatments of the reaction mechanism. They should therefore be viewed with skepticism.

The q_σ^2 dependence of g_{PS} is obtained in accordance with the partially conserved-axial-current (PCAC) hypothesis by assuming pion-pole dominance and the Goldberger-Treiman relation [43,57]. In Eq. (4.5), m_π is the pion mass.

The two-body weak axial charge operator includes a pion-range term, which follows from soft-pion theorem and current algebra arguments [58,59], and short-range terms, associated with scalar- and vector-meson exchanges. The latter are obtained consistently with the two-nucleon interaction model, following a procedure [60] similar to that used to derive the corresponding weak vector-current operators [21]. The two-body axial charge operator due to the N-to-Δ transition has also been included [21,34], although its contribution is found to be very small.

The two-body axial current operators can be divided into two classes: the operators of the first class are derived from π- and ρ-meson exchanges and the $\rho\pi$-transition mechanism. These mesonic operators, first obtained in a systematic way in Ref. [61], give rather small contributions [21]. The operators

in the second class are those that give the dominant two-body contributions, and are due to Δ-isobar excitation [20,21]. We review them here briefly. The N-to-Δ-transition axial current is written as (in the notation of Ref. [21])

$$\mathbf{j}_i^{(1)}(\mathbf{q}; N \to \Delta, A)$$

$$= -\left[g_A^*(q_\sigma^2)\mathbf{S}_i + \frac{g_{PS}^*(q_\sigma^2)}{2\,m\,m_\mu}\mathbf{q}(\mathbf{S}_i \cdot \mathbf{q}) \right] e^{i\mathbf{q}\cdot\mathbf{r}_i} T_{i,\pm} \,, \quad (4.6)$$

where $\mathbf{S}_i$ and $\mathbf{T}_i$ are spin- and isospin-transition operators, which convert a nucleon into a Δ isobar. The induced-pseudoscalar contribution has been obtained from a nonrelativistic reduction of the covariant N-to-Δ-transition axial current [57].

The axial and pseudoscalar form factors g_A^* and g_{PS}^* are parametrized as

$$g_A^*(q_\sigma^2) = R_A\, g_A(q_\sigma^2),$$
$$g_{PS}^*(q_\sigma^2) = -\frac{2\,m_\mu\,m}{m_\pi^2 + q_\sigma^2}\, g_A^*(q_\sigma^2), \quad (4.7)$$

with $g_A(q_\sigma^2)$ given in Eq. (4.4). The parameter R_A is adjusted to reproduce the experimental value of the Gamow-Teller matrix element in tritium β decay (GT$^{\text{EXP}}$), while the q_σ^2 dependence of g_{PS}^* is again obtained by assuming pion-pole dominance and PCAC [43,57]. The value for GT$^{\text{EXP}}$, estimated in Ref. [20], was 0.957(3). This value was determined by assuming $g_A = 1.2654(42)$, $\langle \mathbf{F}\rangle^2 = 0.9987$, where $\langle \mathbf{F}\rangle$ is the reduced matrix element of the Fermi operator $\sum_i \tau_{i,-}$, and the triton half-life $fT_{1/2}$ is (1134.6 ± 3.1) s [62]. We adopt it also in this work, except for the case in which g_A is taken from the PDG, i.e., $g_A = 1.2695(29)$. We then extract GT$^{\text{EXP}} = 0.955(2)$, corresponding to $\langle \mathbf{F}\rangle^2 = 0.999\,26$ and $fT_{1/2} = (1132.1 \pm 4.3)$ s. The new value of $\langle \mathbf{F}\rangle^2$ differs by less than 0.1% from the older value, presumably due to the higher accuracy of the present trinucleon wave functions. The new value of $fT_{1/2}$ has been obtained by averaging the previous value of $fT_{1/2}$ with the new value of Ref. [63] [i.e., (1129.6 ± 3) s], and summing the errors in quadrature. The values for R_A determined in this paper using trinucleon wave functions corresponding to the AV18/UIX are $R_A = 1.21(9)$, when GT$^{\text{EXP}} = 0.957(3)$ and $g_A = 1.2654(42)$, and $R_A = 1.13(6)$, when GT$^{\text{EXP}} = 0.955(2)$ and $g_A = 1.2695(29)$. The experimental error on GT$^{\text{EXP}}$ is responsible for the 5%–8% uncertainty in R_A.

It is important to note that the value of R_A depends on how the Δ-isobar degrees of freedom are treated. In this paper, as in Ref. [34], the two-body Δ-excitation axial operator is derived in the static Δ approximation, using first-order perturbation theory (PT). This approach is considerably simpler than that adopted in Ref. [21], where the Δ degrees of freedom were treated nonperturbatively, within the so-called transition-correlation operator (TCO) approach, by retaining them explicitly in the nuclear wave functions [64]. The results for R_A obtained within the two schemes differ by more than a factor of 2 [21]. However, the results for the observables calculated consistently within the two different approaches are typically within 1% of each other. Finally, because of the procedure adopted to determine R_A, the coupling constant g_A^*

of Eq. (4.7) can not be naively interpreted as the N-to-Δ axial coupling constant. The excitation of additional resonances and their associated contributions will contaminate the value of g_A^*.

The weak vector charge and current operators are constructed from the isovector part of the electromagnetic current, in accordance with the conserved-vector-current hypothesis. The weak charge operator includes the nonrelativistic one-body term and the relativistic spin-orbit and Darwin-Foldy contributions, and is obtained from the corresponding isovector electromagnetic operator, as listed in Ref. [65], by replacing

$$\tau_{i,z}/2 \to \tau_{i,-}. \quad (4.8)$$

Two-body contributions, arising from π- and ρ-meson exchange mechanisms, are also included. Their expressions are listed in Ref. [65], with the substitutions

$$(\boldsymbol{\tau}_i \times \boldsymbol{\tau}_j)_z \to (\boldsymbol{\tau}_i \times \boldsymbol{\tau}_j)_- \quad (4.9)$$

and

$$(\boldsymbol{\tau}_i \times \boldsymbol{\tau}_j)_- = (\boldsymbol{\tau}_i \times \boldsymbol{\tau}_j)_x - i(\boldsymbol{\tau}_i \times \boldsymbol{\tau}_j)_y. \quad (4.10)$$

Electromagnetic form factors are also included, and available parametrizations for them all provide excellent fits of the experimental data at the low-momentum transfer of interest here.

The weak vector current operator retains the one-body operator, two-body "model-independent" (MI) and "model-dependent" (MD) terms, and three-body terms. The MI two-body currents are obtained from the two-nucleon interaction, and by construction satisfy current conservation with it. In this paper, we include the leading two-body "π-like" and "ρ-like" operators, obtained from the isospin-dependent central, spin-spin, and tensor nucleon-nucleon interactions. On the other hand, we have neglected the additional two-body currents arising from nonstatic (momentum-dependent) interactions, since these currents are short ranged, and numerically far less important than those considered here [49]. The MD currents are purely transverse, and therefore cannot be directly linked to the underlying two-nucleon interaction. This calculation includes the isovector currents associated with the $\omega\pi\gamma$ transition mechanism [65], and the excitation of Δ isobars. The former contributions are numerically negligible, while the latter are important in order to reproduce the three-nucleon magnetic moments and elastic form factors [49]. The contributions of the (MD) Δ-isobar currents have been calculated in this case with the TCO method [64], and explicit expressions for these are listed in Ref. [66]. Again, the substitution of Eq. (4.10) is used.

A three-nucleon interaction requires a corresponding three-body current. The latter was first derived in Ref. [49] from a three-nucleon interaction consisting of a dominant two-pion-exchange component, such as the UIX model adopted in this work. The charge-changing three-body (weak vector) current is obtained by applying CVC to the operators listed in Ref. [49], i.e.,

$$\left[\tfrac{1}{2}(\tau_{i,a} + \tau_{j,a} + \tau_{k,a}),\; \mathbf{j}_{ijk,z}^{(3)}(\mathbf{q};\gamma) \right] = i\,\epsilon_{azb}\,\mathbf{j}_{ijk,b}^{(3)}(\mathbf{q};\text{V}), \quad (4.11)$$

TABLE IV. Triton and ^{3}He magnetic moments, in nuclear magnetons, calculated with the AV18/UIX Hamiltonian model and compared with the experimental data. The results labeled IA are obtained with single-nucleon current, while those labeled MI are obtained by including, in addition, the model-independent two-body contributions. The results labeled MD/Δ-PT and MD/Δ-TCO also include the model-dependent contributions, with the Δ-isobar degrees of freedom treated in perturbation theory or within the TCO approach, respectively. Lastly, the results labeled FULL retain three-body contributions. Also shown are the results of Ref. [49].

	^{3}H	^{3}He
IA	2.5745	–1.7634
MI	2.8954	–2.0790
MD/Δ-PT	3.0260	–2.2068
MD/Δ-TCO	2.9337	–2.1079
FULL	2.9525	–2.1299
Ref. [49]	2.953	–2.125
Experiment	2.9790	–2.1276

where $\mathbf{j}_{ijk,z}^{(3)}(\mathbf{q}; \gamma)$ are the isovector three-body electromagnetic currents, and $a, b = x, y, z$ are isospin Cartesian components.

We conclude by emphasizing that the model for the weak transition operator is the same as that of Ref. [34], except for two differences relative to its vector component: (i) the MD two-body currents due to Δ-isobar degrees of freedom are treated nonperturbatively with the TCO method, rather than in first-order PT, and (ii) three-body terms are also included (they were neglected in Ref. [34]). As shown in Table IV, the present model for the electromagnetic current provides an excellent description of the trinucleon magnetic moments, in particular of their isovector contribution, to better than 1% (row labeled with "FULL"). This gives us confidence in the accuracy of the corresponding weak vector currents. We also note that (i) three-body contributions are important to achieve this level of agreement between theory and experiment; (ii) the results obtained with the model of Ref. [34], labeled by MD/Δ-PT, are at variance with data at the 3% level; (iii) the difference between the present "FULL" results and those of Ref. [49] can be traced back to the fact that here we have used slightly more accurate wave functions, with a careful treatment of $T = 3/2$ components. However, we should note that, in contrast to Ref. [49], MI two-body contributions arising from nonstatic components of the two-nucleon interaction have been ignored. They amount to a negligible 0.1% correction.

B. The chiral effective field theory approach

The χEFT weak transition operator is taken from Refs. [22] and [41], where it was derived in covariant perturbation theory based on the heavy-baryon formulation of chiral Lagrangians by retaining corrections up to N3LO. It was recently used in Ref. [67] to study electromagnetic $M1$ transitions. Before reviewing its main features in the following, we note that the kinematical regime relevant in muon capture, where the momentum transfer is of the order of the muon mass, is different from that of the threshold processes to which it

has been applied so far. From this perspective, it would be interesting to investigate contributions beyond N3LO in order to assess the convergence pattern of the chiral expansion in the present context. However, this issue will not be discussed further in this paper.

The vector and axial-vector one-body operators are the same as those obtained within the SNPA, and described in Sec. IV A. These one-body operators are also listed in Eq. (17) of Ref. [22], except that we also include corrections in the vector current, which arise when the nonrelativistic reduction is carried out to next-to-leading order (proportional to $1/m^3$). The resulting operator is given (in momentum space) by

$$\mathbf{j}_i^{(1)}(\mathbf{q}; V) = \mathbf{j}_i^{(1)NR}(\mathbf{q}; V) + \mathbf{j}_i^{(1)RC}(\mathbf{q}; V), \quad (4.12)$$

where $\mathbf{j}_i^{(1)NR}(\mathbf{q}; V)$ is the standard leading-order term

$$\mathbf{j}_i^{(1)NR}(\mathbf{q}; V) = \frac{1}{m}\tau_{i,-}\left[G_E^V(q_\sigma^2)\mathbf{k} + iG_M^V(q_\sigma^2)\boldsymbol{\sigma}_i \times \mathbf{q}\right], \quad (4.13)$$

and $\mathbf{j}_i^{(1)RC}(\mathbf{q}; V)$ is

$$\begin{aligned}
\mathbf{j}_i^{(1)RC}(\mathbf{q}; V) = &-\frac{1}{4m^3}\tau_{i,-}\big(G_E^V(q_\sigma^2)\,\mathbf{k}^2(2\mathbf{k} + i\boldsymbol{\sigma}_i \times \mathbf{q}) \\
&+ i\big[G_M^V(q_\sigma^2) - G_E^V(q_\sigma^2)\big] \\
&\times (2\mathbf{k}\cdot\mathbf{q}\,\boldsymbol{\sigma}_i \times \mathbf{k} + \mathbf{k}\times\mathbf{q}\,\boldsymbol{\sigma}_i\cdot\mathbf{k})\big). \quad (4.14)
\end{aligned}$$

In these equations, $\mathbf{k} = (\mathbf{p}_i' + \mathbf{p}_i)/2$, $\mathbf{q} = \mathbf{p}_i' - \mathbf{p}_i$, with $\mathbf{p}_i'$ and $\mathbf{p}_i$ momenta of the outgoing and ingoing nucleons, respectively, and $G_E^V(q_\sigma^2)$ and $G_M^V(q_\sigma^2)$ denote the isovector combinations of the nucleon electric and magnetic form factors [65]. Note that Eqs. (4.12)–(4.14) can also be obtained from Eq. (11) of Ref. [41], with the substitution (4.8) required by CVC.

The axial two-body charge and currents are from Ref. [22]. In particular, the axial charge operator is that derived originally in Ref. [58]. In the SNPA, additional contributions are considered, which, in a χEFT context, are expected to appear at higher orders. The two-body axial-current operator consists of two contributions: a one-pion exchange term and a (nonderivative) two-nucleon contact term. The explicit expressions for these terms can be found in Ref. [22]. While the coupling constants that appear in the one-pion exchange term are fixed by πN data, the low-energy constant (LEC) d_R, determining the strength of the contact term, has been fixed by reproducing GT$^{\text{EXP}}$. The value $g_A = 1.2654(42)$ has been used. The values for d_R are presented in Table V and discussed below.

The two-body vector currents are decomposed into four terms [41]: the soft-one-pion-exchange (1π) term, vertex corrections to the one-pion exchange ($1\pi C$), the two-pion exchange (2π), and a contact-term contribution. Their explicit expressions can be found in Eqs. (12)–(18) of Ref. [41], with the replacements (4.3) and (4.10) in the isospin operators. All the 1π, $1\pi C$ and 2π contributions contain LECs estimated in Ref. [68], using resonance-saturation arguments. The contact-term electromagnetic contribution is given by

$$\begin{aligned}
\mathbf{j}_{ij}^{(2)CT}(\mathbf{q}; \gamma) = &-\frac{i}{2m}e^{i\mathbf{q}\cdot\mathbf{R}}\mathbf{q} \times \big[\,g_{4S}(\boldsymbol{\sigma}_i + \boldsymbol{\sigma}_j) \\
&+ g_{4V}(\boldsymbol{\tau}_i \times \boldsymbol{\tau}_j)_z\boldsymbol{\sigma}_i \times \boldsymbol{\sigma}_j\big]\delta_\Lambda(r). \quad (4.15)
\end{aligned}$$

TABLE V. The LECs g_{4S} and g_{4V} associated with the isoscalar and isovector contact terms in the electromagnetic current [see Eq. (4.15)], and the LEC d_R of the two-body axial-current contact term, calculated for three values of the cutoff Λ with triton and ^{3}He wave functions obtained from the AV18/UIX model. For $\Lambda = 600$ MeV, the N3LO/N2LO model is also used.

	Λ (MeV)	g_{4S}	g_{4V}	d_R
AV18/UIX	500	0.69(1)	2.065(6)	0.97(7)
	600	0.55(1)	0.793(6)	1.75(8)
	800	0.25(2)	−1.07(1)	3.89(10)
N3LO/N2LO	600	0.11(1)	3.124(6)	1.00(9)

The function $\delta_\Lambda(r)$, as well as the Yukawa functions that appear in the 1π, $1\pi C$, and 2π operators and in the two-body axial-current terms, are obtained by performing the Fourier transform from momentum to coordinate space with a Gaussian regulator characterized by a cutoff Λ. This cutoff determines the momentum scale below which these EFT currents are expected to be valid, i.e., $\Lambda = 500 - 800$ MeV [22]. The explicit expression of $\delta_\Lambda(r)$ in Eq. (4.15) is

$$\delta_\Lambda(r) = \int \frac{d\mathbf{k}^3}{(2\pi)^3} e^{-k^2/\Lambda^2} e^{i\mathbf{k}\cdot\mathbf{r}}. \qquad (4.16)$$

The coefficients g_{4S} and g_{4V} of Eq. (4.15) are fixed to reproduce the experimental values of triton and ^{3}He magnetic moments for each nuclear interaction and cutoff value. This procedure is similar to that used to fix the strength d_R of the contact term in the two-body axial current discussed previously. The results are presented in Table V. A few comments are in order: (i) while values of both g_{4S} and g_{4V} are presented, only g_{4V} is relevant in this work, since CVC relates the isovector electromagnetic current to the weak vector current. (ii) The uncertainty on g_{4S} and g_{4V} is not due to the experimental errors on the triton and ^{3}He magnetic moments, which are, in fact, negligible, but rather to numerics. We have used a random walk consisting of 1.6 million configurations in order to reduce the numerical uncertainty on $\Delta\mu$, the difference between the experimental magnetic moments and the result obtained without the contact contributions, to less than 1%. In contrast, the experimental

error on GT$^{\text{EXP}}$ is primarily responsible for the uncertainty in d_R. (iii) The values reported for d_R are different, but consistent within the error, with those listed in Table II of Ref. [22]. This is due to differences between the present ^{3}H and ^{3}He wave functions and those of Ref. [22] (we have already commented on this in the previous section). (iv) The g_{4S} and g_{4V} values are rather different from those listed in Ref. [67]. We observe that g_{4S} and g_{4V} are fixed by fitting very small quantities. In the AV18/UIX case with $\Lambda = 600$ MeV, for instance, the value $\Delta\mu$ is 0.0461(4) for triton and –0.0211(4) for ^{3}He, where the uncertainties are statistical errors due to the Monte Carlo integrations. Consequently, the resulting values will be sensitive to several factors, including numerics. However, it is worthwhile to point out that the isovector contact contribution to the muon-capture rates under consideration turns out to be negligible. Finally, we should point out that the χEFT model for the weak vector current operator differs in some of its two-pion exchange parts from that obtained in time-ordered perturbation theory by some of the present authors in Ref. [69]. The origins of these differences have been discussed in Refs. [69,70]. However, for consistency with the calculations of the pp and hep reactions of Ref. [22], we have chosen to use the χEFT model illustrated above. We do not expect these differences to be numerically significant for the processes under consideration.

V. RESULTS

The results for the total rates of muon capture on deuteron and ^{3}He are presented in the following two subsections.

A. Muon capture on deuteron

In a partial-wave expansion of the final nn state, all channels with total angular momentum $J \leqslant 2$ and relative orbital angular momentum $L \leqslant 3$ have been included, i.e., $^1S_0$, $^3P_0$, $^3P_1$, $^3P_2$, $^1D_2$, and $^3F_2$. Partial waves of higher order contribute less than $\simeq 0.5$ % to the rate. Indeed, the $^3F_2$ contribution turns out to be already below this level.

We present in Table VI the results for the total capture rate in the doublet hyperfine state. Both models for the nuclear weak transition operator presented in Secs. IV A and IV B have been used, labeled SNPA and EFT*, respectively. The nuclear wave functions have been calculated with the AV18 [23] or the

TABLE VI. Total rate for muon capture on deuteron, in the doublet initial hyperfine state, in s^{-1}. The different partial-wave contributions are indicated. The numbers within parentheses indicate the theoretical uncertainty arising from the adopted fitting procedures, as explained in Sec. IV. Such uncertainty is not indicated when less than 0.1 s^{-1}. The label SNPA indicates that the results have been obtained using the model for the weak transition operator of Sec. IV A, while the label EFT* indicates that the model of Sec. IV B is used. The AV18 and N3LO interactions have been used to calculate the deuteron and nn wave functions.

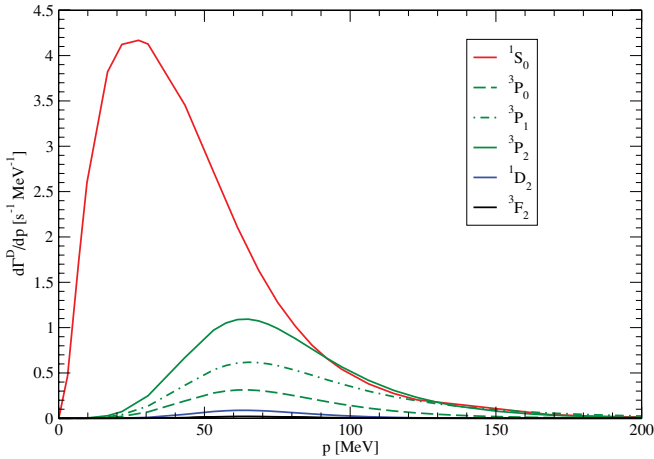|		$^1S_0$	$^3P_0$	$^3P_1$	$^3P_2$	$^1D_2$	$^3F_2$	Total
SNPA (AV18)	$g_A = 1.2654(42)$	246.6(7)	20.1	46.7	71.6	4.5	0.9	390.4(7)
	$g_A = 1.2695(29)$	246.8(5)	20.1	46.8	71.8	4.5	0.9	390.9(7)
EFT* (AV18)	$\Lambda = 500$ MeV	250.0(8)	19.9	46.2	71.2	4.5	0.9	392.7(8)
	$\Lambda = 600$ MeV	250.0(8)	19.8	46.3	71.1	4.5	0.9	392.6(8)
	$\Lambda = 800$ MeV	249.7(7)	19.8	46.4	71.1	4.5	0.9	392.4(7)
EFT* (N3LO)	$\Lambda = 600$ MeV	250.5(7)	19.9	46.4	71.5	4.4	0.9	393.6(7)

FIG. 1. (Color online) Differential capture rate $d\Gamma^D/dp$, defined in Eq. (2.21), as a function of the *nn* relative momentum p in MeV. The calculation is performed with the SNPA (AV18) model.

N3LO [39] two-nucleon interaction. The label EFT* is used to denote the results of calculations in which the matrix elements of χEFT weak operators are evaluated between wave functions corresponding to both conventional and chiral potentials. The first approach (based on a conventional potential) is often referred to in the literature as the "hybrid" approach. The second, using chiral potentials and currents, is, in principle, a full-fledged χEFT calculation, except that these potentials and currents have not (yet) been derived consistently at the same order in the low-momentum scale. For this reason, we characterize the corresponding results with the EFT* label.

Within each Hamiltonian model, the parameters present in the SNPA and EFT* axial-current models have been fitted to reproduce GT^{EXP} in tritium β decay, as discussed in Sec. IV. Furthermore, the LECs in the EFT* weak vector current have been fitted to reproduce the $A = 3$ magnetic moments. The three-nucleon wave functions have been generated, in this fitting procedure, from two- and three-nucleon interactions, either AV18 and UIX [36], or N3LO and N2LO [40]. Inspection of Table VI shows that the $^1S_0$ contribution is the leading one, but $L \geqslant 1$ contributions are significant and account for $\sim$37% of the total rate. By comparison between the first and second rows of the table, we conclude that there is no difference in the results, within uncertainties, when the older value for g_A, $g_A = 1.2654(42)$, or the most recent one, $g_A = 1.2695(29)$, is used. This reflects the fact that the factor R_A (see Sec. IV A) has been constrained by GT^{EXP} in both cases. The model dependence due to interactions, currents, and the cutoff Λ (present in the χEFT version of these currents) is at the 1% level in the total rate and hence very weak. It is a bit larger, i.e., 2%, in the $^1S_0$ channel, for which two-body current contributions are larger (see Tables VII and VIII) . In conclusion, a total capture rate in the range

$$\Gamma^D = (389.7 - 394.3)\,\text{s}^{-1} \qquad (5.1)$$

can be conservatively ascribed to reaction (1.1). This result is in agreement with the measurements of Refs. [5,6,8], but not with that of Ref. [7]. The differences with the theoretical results of Refs. [16–18] are also very small. In particular, the

TABLE VII. Cumulative contributions to the total rate for muon capture on deuteron in s^{-1}, when the model of Sec. IV A is used for the weak transition operator. The deuteron and *nn* wave functions are calculated using the AV18 interaction. Only the $^1S_0$ and $^3P_2$ partial waves are considered, since they give the leading contributions. The labels IA + RC, PS, and Mesonic indicate the results obtained by retaining the impulse approximation plus relativistic corrections, the induced-pseudoscalar, and the purely mesonic contributions. The label Δ-PT(A-w/o PS) is used to indicate that the axial charge and current contributions due to Δ isobars are retained perturbatively, but the induced-pseudoscalar contribution in the one-body Δ current is not included, while the label Δ-PT(A-w PS) is used when the N-to-Δ induced-pseudoscalar contribution is also included. Finally, the labels Δ-PT(V) and Δ-TCO(V) are used when the vector-current contributions due to Δ isobars are treated perturbatively and within the TCO scheme, respectively. The value $g_A = 1.2654(42)$ is used. The numbers in parentheses indicate the theoretical errors arising from the fitting procedure adopted for R_A. This uncertainty is not shown if less than 0.1 s^{-1}.

	$^1S_0$	$^3P_2$
IA + RC	293.0	82.6
PS	233.2	71.6
Mesonic	237.5	71.4
Δ-PT(A-w/o PS) + Δ-PT(V)	248.3(8)	71.6
Δ-PT(A-w/o PS) + Δ-TCO(V)	247.7(8)	71.6
Δ-PT(A-w PS) + Δ-TCO(V)	246.6(7)	71.6

authors of Ref. [18] find that $\Gamma^D(^1S_0) = 245$ s^{-1}, in contrast to the $\Gamma^D(^1S_0) = 250$ s^{-1} reported here. We have explicitly verified that this difference is mainly due to the inclusion in this work of mesonic two-body contributions in the weak vector current beyond the soft-one-pion-exchange term discussed in Sec. IV B. On the other hand, the results of Refs. [15,19] are significantly larger than those listed here, presumably because these authors have not constrained their weak current to reproduce GT^{EXP} and the isovector magnetic moment of the trinucleons. We observe that our approach also provides a value for muon capture on ^{3}He in excellent agreement with the experimental data.

For future reference, we show, in Fig. 1, the differential capture rate $d\Gamma^D/dp$, defined in Eq. (2.21), as function of the *nn* relative momentum p, calculated with the SNPA (AV18) model. Integrating each partial-wave contribution leads to the values listed in the first row of Table VI.

The cumulative contributions to the leading $^1S_0$ and $^3P_2$ capture rates of various terms in the nuclear current operator are given in Table VII for the SNPA and in Table VIII for the EFT*. Table VII shows that (i) the (one-body) induced-pseudoscalar contribution is significant, as expected, and reduces the rate of $\sim$20% ($\sim$13%) in $^1S_0$ ($^3P_2$) capture; (ii) the mesonic contributions are very small; (iii) the Δ-isobar contributions are significant only in *S*-wave capture, and differences in the vector two-body current originating from treating the Δ-isobar degrees of freedom either perturbatively or within the TCO approach are negligible; (iv) the Δ-isobar induced pseudoscalar axial-current contribution of Eqs. (4.6) and (4.7) is of the order of 1 s^{-1} for $^1S_0$ capture.

TABLE VIII. Same as Table VII, but with the nuclear current model of Sec. IV B. The labels IA + RC, PS, and Mesonic indicate the results obtained by retaining the impulse approximation plus relativistic corrections, the induced-pseudoscalar, and the mesonic contributions. The relativistic corrections to the one-body vector current operator include the additional terms of Eq. (4.14). The numbers in parentheses indicate the theoretical errors arising from the fitting procedure adopted for d_R and g_{4V}. This uncertainty is not shown if less than 1 s^{-1}.

		$^1S_0$	$^3P_2$
$\Lambda = 500$ MeV	IA + RC	292.5	82.5
	PS	232.7	71.6
	Mesonic	250.0(8)	71.2
$\Lambda = 600$ MeV	IA + RC	292.5	82.5
	PS	232.7	71.6
	Mesonic	250.0(8)	71.1
$\Lambda = 800$ MeV	IA + RC	292.5	82.5
	PS	232.7	71.6
	Mesonic	249.7(7)	71.1

From inspection of Table VIII, we can conclude the following. (i) The one-body contributions (labeled IA + RC and PS) are slightly different from those reported in the SNPA. While the EFT* one-body axial charge and current, and vector charge, operators are the same as in the SNPA, the EFT* one-body vector current includes the relativistic corrections of Eq. (4.14), ignored in the SNPA. On the other hand, the differences between SNPA and EFT* one-body contributions remain well below the 1% level, and therefore within the theoretical uncertainty. However, it would be interesting to study the contributions of these relativistic corrections to the many electromagnetic observables analyzed within the SNPA over the years [49,50]. A first step in this direction has been done in Ref. [71]. (ii) The Λ dependence is very weak, well below the 1% level. (iii) The $^3P_2$ term does not show any Λ dependence nor any sensitivity to the d_R and g_{4V} fitting procedure. This is easily understood by observing that the contact terms in the vector and axial currents are proportional to $(\boldsymbol{\tau}_i \times \boldsymbol{\tau}_j)_-(\boldsymbol{\sigma}_i \times \boldsymbol{\sigma}_j)$ [see Ref. [22] and Eq. (4.15)], the matrix elements of which vanish when calculated between the deuteron state and ^3P_J nn states.

By comparison of the results listed in Tables VII and VIII, we observe that the main source for the 2% theoretical uncertainty in the $^1S_0$ channel quoted above is the Δ-isobar induced-pseudoscalar contribution; if it were neglected, the SNPA and EFT* $^1S_0$ results would agree at the 1% level. We observe that the strength of the associated operator, which is only included in the SNPA calculation and plays no role in tritium β decay (being proportional to the momentum transfer $\mathbf{q}$), follows from PCAC and pion-dominance arguments (see Sec. IV A).

B. Muon capture on ^{3}He

We present in Table IX the results for the total capture rate Γ_0 defined in Eq. (2.19). The theoretical uncertainties due to the fitting procedure of R_A (SNPA) or d_R and g_{4V} (EFT*)

TABLE IX. Total rate for muon capture on ^{3}He in s^{-1}. The numbers in parentheses indicate the theoretical uncertainties due to the adopted fitting procedure (see Sec. IV). The label SNPA (EFT*) indicates that the results have been obtained using the model for the weak transition operator of Sec. IV A (Sec. IV B). The triton and ^{3}He wave functions are obtained from the AV18/UIX and N3LO/N2LO Hamiltonians.

		Γ_0
SNPA (AV18/UIX)	$g_A = 1.2654(42)$	1486(8)
	$g_A = 1.2695(29)$	1486(5)
EFT* (AV18/UIX)	$\Lambda = 500$ MeV	1487(8)
	$\Lambda = 600$ MeV	1488(9)
	$\Lambda = 800$ MeV	1488(8)
EFT* (N3LO/N2LO)	$\Lambda = 600$ MeV	1480(9)
Experiment		1496(4)

are in parentheses. The results in the first two rows have been obtained in the SNPA, using the AV18/UIX Hamiltonian and the two available values for g_A. These results are the same, since a change in g_A is compensated by a corresponding one in R_A. The results of the next three rows have been obtained within the hybrid approach EFT* (AV18/UIX). They show a very weak Λ dependence, and are in excellent agreement with those reported in SNPA. The result in the last row is with the EFT* (N3LO/N2LO). The EFT* (AV18/UIX) and EFT* (N3LO/N2LO) differ by 8 s^{-1}, or less than 1%. In view of this, we quote conservatively a total capture rate for reaction (1.2) in the range

$$\Gamma_0 = (1471 - 1497) \text{ s}^{-1} , \qquad (5.2)$$

by keeping the lowest and upper bounds in the values of Table IX.

The contributions of the different components of the weak current and charge operators to the total rate and to the reduced matrix elements of the contributing multipoles are reported in Table X for SNPA and Table XI for EFT*. The HH wave functions have been calculated using the AV18/UIX Hamiltonian model. In Table X, R_A has been fixed to its central value 1.21, and in Table XI we use $\Lambda = 600$ MeV and consequently $d_R = 1.75$ and $g_{4V} = 0.793$ (see Table V). The notation in these tables is the same as that of Tables VII and VIII of Sec. V A, with the only exception of the label Δ-TCO(V), which here indicates that the two-body Δ currents are treated with the TCO method, and that the three-body current, constructed consistently with the UIX three-nucleon interaction, are also included. In Table X, we observe that the induced-pseudoscalar term gives a significant contribution to the $L_1(A)$ and $C_1(A)$ RMEs, although the latter is much smaller than $L_1(A)$ in magnitude. The mesonic contributions to $C_0(V)$, $C_1(A)$, $L_1(A)$, and $E_1(A)$ are small, while they provide a 15% correction to $M_1(V)$, as expected (in the isovector magnetic moments of the trinucleons, these mesonic currents give a 15% contribution relative to the one body). Contributions due to Δ isobar excitations in the weak vector and axial currents are at the few percent level. We note that the result for Γ_0 is in excellent agreement with

TABLE X. Cumulative contributions to the total rate Γ_0 for muon capture on ^{3}He, in s^{-1}, and to the reduced matrix elements (RMEs) $C_0(V)$, $C_1(A)$, $L_1(A)$, $E_1(A)$, and $M_1(V)$ (see Sec. II), when the model of Sec. IV A is used for the weak transition operator ($R_A = 1.21$). The HH wave functions have been calculated using the AV18/UIX Hamiltonian. Notation is the same as in Table VII, except for Δ-TCO(V), which here is used to indicate that the Δ-isobar contributions are treated with the TCO method, and, in addition, three-body weak vector-current contributions are included. Note that $C_0(V)$ is purely real, while the other RMEs are purely imaginary.

	Γ_0	$C_0(V)$	$C_1(A)$	$L_1(A)$	$E_1(A)$	$M_1(V)$
IA + RC	1530	–0.3287	0.7440×10^{-2}	–0.4056	–0.5516	0.1127
PS	1316		0.3986×10^{-2}	–0.2589		
Mesonic	1385	–0.3283	0.4024×10^{-2}	–0.2619	–0.5562	0.1315
Δ-PT(A-w/o PS) + Δ-PT(V)	1501		0.4287×10^{-2}	–0.2811	–0.5821	0.1370
Δ-PT(A-w/o PS) + Δ-TCO(V)	1493					0.1376
Δ-PT(A-w PS) + Δ-TCO(V)	1486			–0.2742		

that of the earlier study of Ref. [34]. This agreement comes about because of two compensating effects. On one hand, the $L_1(A)$ and $E_1(A)$ RMEs are, in magnitude, slightly larger, as a consequence of the fact that the parameter R_A is slightly larger here than in Ref. [34], because of the more accurate wave functions employed. On the other hand, the $M_1(V)$ RME corresponding to Δ-TCO(V) is slightly smaller than that calculated in Ref. [34], i.e., $M_1(V) = 0.1355$ in Ref. [34] versus $M_1(V) = 0.1346$. This last value results from dividing the value listed in Table X by the factor 1.022, arising from the normalization correction of the trinucleon wave functions due to the presence of explicit Δ-isobar degrees of freedom, i.e., $N_\Delta = \sqrt{\langle \Psi_{N+\Delta} | \Psi_{N+\Delta} \rangle / \langle \Psi_{N\text{only}} | \Psi_{N\text{only}} \rangle}$, where $\Psi_{N+\Delta}$ ($\Psi_{N\text{only}}$) is the nuclear wave function with both nucleon and Δ (nucleon only) degrees of freedom. Indeed, the Δ-TCO(V) $M_1(V)$ RME should be compared with $M_1(V)$ corresponding to Δ-PT(V) in Table X.

In Table XI, we observe the following: (i) the one-body vector-current contribution to the $M_1(V)$ RME is different than in SNPA. This is due to the presence of the additional relativistic corrections of Eq. (4.14). (ii) The mesonic contributions are significant for the $L_1(A)$, $E_1(A)$, and $M_1(V)$ RMEs, and bring their values closer to those in the SNPA. (iii) The $1\pi C$, 2π, and contact terms in the mesonic vector current are important. If they were to be neglected, the total $M_1(V)$ RME would be equal to 0.1201 and consequently $\Gamma_0 = 1453$ s^{-1}. (iv) The results of Table XI should be compared with those of Table 2 of Ref. [37]. We find significant differences in all the RMEs, both for the one-body contribution (here labeled PS and in Ref. [37] IA) and the complete calculation. Only the results for the $M_1(V)$ RME appear to be similar to each other, although it is unclear whether in Ref. [37] the vector $1\pi C$, 2π, and contact-term contributions are included.

TABLE XI. Same as Table X, but with the nuclear current model of Sec. IV B. The value for the cutoff Λ has been fixed to 600 MeV, and $d_R = 1.75$ and $g_{4V} = 0.793$. Notation is the same as in Table VIII.

	Γ_0	$C_0(V)$	$C_1(A)$	$L_1(A)$	$E_1(A)$	$M_1(V)$
IA + RC	1517	–0.3287	0.7440×10^{-2}	–0.4056	–0.5516	0.1082
PS	1303		0.3986×10^{-2}	–0.2589		
Mesonic	1488		0.3978×10^{-2}	–0.2810	–0.5833	0.1317

Finally, we observe that when the N3LO/N2LO Hamiltonian model is used, $C_0(V)$, $C_1(A)$, $L_1(A)$, $E_1(A)$, and $M_1(V)$ are –0.3288, 0.4130×10^{-2}, –0.2773, –0.5810, and 0.1329, respectively, when the mesonic contributions are included. Comparing these results with the AV18/UIX results of Table XI, we see that all the RMEs are comparable at the 1% level. This fact is reflected in the ~1% difference between the AV18/UIX and N3LO/N2LO results for Γ_0. Therefore, it does not seem possible to identify a particular source for this 1% difference.

VI. SUMMARY AND CONCLUSIONS

Total rates for muon capture on deuteron and ^{3}He have been calculated within a consistent approach, based on realistic interactions and weak currents consisting of vector and axial-vector components with one- and many-body terms. Two different approaches have been used to derive these operators. The first one goes beyond the impulse approximation by including meson-exchange-current contributions and terms arising from the excitation of Δ-isobar degrees of freedom. This approach, labeled SNPA, has been widely and successfully used in studies of electroweak processes (see, for instance, Refs. [20,21,34,46,49]). The second approach, labeled EFT*, includes two-body contributions, beyond the impulse approximation, derived within a systematic χEFT expansion, up to N3LO. The only parameter in the SNPA nuclear weak current model is present in the axial current and is determined by fitting the experimental value for the triton half-life. In the case of the EFT* approach, two LECs appear, one in the vector and one in the axial-vector component (note that the LEC appearing in the isoscalar electromagnetic contact term does not contribute here). They are fixed to reproduce, respectively, the $A = 3$ isovector magnetic moment and triton half-life.

Our final results are summarized in Eqs. (5.1) and (5.2). The very accurate experimental datum of Ref. [14] for the total rate in muon capture on ^{3}He is very well reproduced. For the muon capture on deuteron, a precise measurement should become available in the near future [9]. The dependence of the results on the input Hamiltonian model, or on the model for the nuclear transition operator, is weak, at less than the 1% level. This weak model dependence is a

consequence of the procedure adopted to constrain the weak current.

We conclude by noting the following. (i) Within the EFT* approach, the two-body vector-current operators beyond the one-pion-exchange term give significant contributions to the total rate, especially for muon capture on ^{3}He. These terms have been included in the study of weak processes here for the first time. However, since they are proportional to the momentum transfer, their contribution is expected to be negligible in the pp and hep reactions [22]. (ii) Some of the radiative corrections are accounted for in these predictions for the muon rates, since the value adopted for the Fermi coupling constant G_V is that extracted from an analysis of superallowed β decays [44]. The size of these corrections (roughly 2.4% on G_V^2) is in agreement with that calculated independently in Ref. [72] for the muon capture on hydrogen and helium. The additional radiative corrections, originating from vacuum polarization effects on the muon bound-state wave function, have also been estimated by the authors of Ref. [72]. In the case of the muon capture on ^{3}He, they increase the predicted rates by about 0.68%, leading to 1496 s^{-1} for the AV18/UIX model, and to 1490 s^{-1} for the EFT*(N3LO/N2LO) model, and thus bringing them into closer agreement with experiment. (iii) The

value for the induced-pseudoscalar coupling used in this study, $g_{PS} = -8.28$ at the four-momentum transfer relevant for muon capture on ^{3}He ($q_\sigma^2 = 0.954m_\mu^2$), is consistent with that predicted by PCAC and chiral perturbation theory [73]. The agreement between the calculated and experimental muon capture rates confirms the validity of these predictions. (iv) The agreement between our final results for the muon capture rate on ^{3}He and those of Ref. [37] confirms the tight limits obtained there on possible contributions from second-class currents.

Finally, we remark that it would be interesting to extend these calculations to the processes $\mu^- + {}^3\text{He} \rightarrow n + d + \nu_\mu$ and $\mu^- + {}^4\text{He} \rightarrow n + {}^3\text{H} + \nu_\mu$, for which experimental data are also available [12,74,75].

ACKNOWLEDGMENTS

[1] D. F. Measday, Phys. Rep. **354**, 243 (2001).

[2] T. Gorringe and H. W. Fearing, Rev. Mod. Phys. **76**, 31 (2004).

[3] S. Vaintraub, N. Barnea, and D. Gazit, Phys. Rev. C **79**, 065501 (2009); E. O'Connor, D. Gazit, C. J. Horowitz, A. Schwenk, and N. Barnea, *ibid.* **75**, 055803 (2007); D. Gazit and N. Barnea, Phys. Rev. Lett. **98**, 192501 (2007).

[4] E. G. Adelberger *et al.*, arXiv:1004.2318.

[5] I.-T. Wang *et al.*, Phys. Rev. **139**, B1528 (1965).

[6] A. Bertin *et al.*, Phys. Rev. D **8**, 3774 (1973).

[7] G. Bardin *et al.*, Nucl. Phys. A **453**, 591 (1986).

[8] M. Cargnelli *et al.*, *Workshop on Fundamental μ Physics*, Los Alamos, 1986, LA 10714C; *Nuclear Weak Process and Nuclear Structure, Yamada Conference XXIII*, edited by M. Morita, H. Ejiri, H. Ohtsubo, and T. Sato (World Scientific, Singapore, 1989), p. 115.

[9] V. A. Andreev *et al.* (MuSun Collaboration) [http://www.npl.illinois.edu/exp/musun] (2007).

[10] I. V. Falomkin *et al.*, Phys. Lett. **3**, 229 (1963).

[11] O. A. Zaimidoroga *et al.*, Phys. Lett. **6**, 100 (1963).

[12] L. B. Auerbach *et al.*, Phys. Rev. **138**, B127 (1965).

[13] D. R. Clay, J. W. Keuffel, R. L. Wagner, and R. M. Edelstein, Phys. Rev. **140**, B587 (1965).

[14] P. Ackerbauer *et al.*, Phys. Lett. B **417**, 224 (1998).

[15] J. Adam and E. Truhlik, Nucl. Phys. A **507**, 675 (1990).

[16] N. Tatara, Y. Kohyama, and K. Kubodera, Phys. Rev. C **42**, 1694 (1990).

[17] M. Doi *et al.*, Nucl. Phys. A **511**, 507 (1990); M. Doi *et al.*, Prog. Theor. Phys. **86**, 13 (1991).

[18] S. Ando *et al.*, Phys. Lett. B **533**, 25 (2002).

[19] P. Ricci, E. Truhlik, B. Mosconi, and J. Smejkal, Nucl. Phys. A **837**, 110 (2010).

[20] R. Schiavilla *et al.*, Phys. Rev. C **58**, 1263 (1998).

[21] L. E. Marcucci, R. Schiavilla, M. Viviani, A. Kievsky, and S. Rosati, Phys. Rev. Lett. **84**, 5959 (2000); L. E. Marcucci,

R. Schiavilla, M. Viviani, A. Kievsky, S. Rosati, and J. F. Beacom, Phys. Rev. C **63**, 015801 (2000).

[22] T.-S. Park *et al.*, Phys. Rev. C **67**, 055206 (2003).

[23] R. B. Wiringa, V. G. J. Stoks, and R. Schiavilla, Phys. Rev. C **51**, 38 (1995).

[24] V. G. J. Stoks, R. A. M. Klomp, C. P. F. Terheggen, and J. J. de Swart, Phys. Rev. C **49**, 2950 (1994).

[25] J.-W. Chen, T. Inoue, X. Ji, and Y. Li, Phys. Rev. C **72**, 061001(R) (2005).

[26] J. G. Congleton and H. W. Fearing, Nucl. Phys. A **552**, 534 (1992).

[27] J. G. Congleton and E. Truhlik, Phys. Rev. C **53**, 956 (1996).

[28] R. B. Wiringa, R. A. Smith, and T. L. Ainsworth, Phys. Rev. C **29**, 1207 (1984).

[29] S. A. Coon *et al.*, Nucl. Phys. A **317**, 242 (1979).

[30] E. C. Y. Ho, H. W. Fearing, and W. Schadow, Phys. Rev. C **65**, 065501 (2002).

[31] W. N. Cottingham *et al.*, Phys. Rev. D **8**, 800 (1973).

[32] R. Machleidt, K. Holinde, and Ch. Elster, Phys. Rep. **149**, 1 (1987); R. Machleidt, Adv. Nucl. Phys. **19**, 189 (1989).

[33] R. Machleidt, Phys. Rev. C **63**, 024001 (2001).

[34] L. E. Marcucci, R. Schiavilla, S. Rosati, A. Kievsky, and M. Viviani, Phys. Rev. C **66**, 054003 (2002).

[35] A. Kievsky *et al.*, J. Phys. G: Nucl. Part. Phys. **35**, 063101 (2008).

[36] B. S. Pudliner, V. R. Pandharipande, J. Carlson, and R. B. Wiringa, Phys. Rev. Lett. **74**, 4396 (1995).

[37] D. Gazit, Phys. Lett. B **666**, 472 (2008).

[38] N. Barnea, W. Leidemann, and G. Orlandini, Phys. Rev. C **61**, 054001 (2000); N. Barnea, W. Leidemann, and G. Orlandini, Nucl. Phys. A **693**, 565 (2001); N. Barnea and A. Novoselsky, Ann. Phys. (NY) **256**, 192 (1997).

[39] D. R. Entem and R. Machleidt, Phys. Rev. C **68**, 041001 (2003).

[40] P. Navrátil, Few-Body Syst. **41**, 117 (2007).

[41] Y.-H. Song, R. Lazauskas, and T.-S. Park, Phys. Rev. C **79**, 064002 (2009).

[42] E. Epelbaum, U.-G. Meissner, and W. Glockle, Nucl. Phys. A **747**, 362 (2005).

[43] J. D. Walecka, *Theoretical Nuclear and Subnuclear Physics* (Oxford University Press, New York, 1995).

[44] J. C. Hardy *et al.*, Nucl. Phys. A **509**, 429 (1990).

[45] M. Viviani *et al.*, Few-Body Syst. **39**, 159 (2006).

[46] L. E. Marcucci, A. Kievsky, L. Girlanda, S. Rosati, and M. Viviani, Phys. Rev. C **80**, 034003 (2009).

[47] W. Kohn, Phys. Rev. **74**, 1763 (1948).

[48] R. Schiavilla and R. B. Wiringa, Phys. Rev. C **65**, 054302 (2002).

[49] L. E. Marcucci, M. Viviani, R. Schiavilla, A. Kievsky, and S. Rosati, Phys. Rev. C **72**, 014001 (2005).

[50] L. E. Marcucci, M. Pervin, S. C. Pieper, R. Schiavilla, and R. B. Wiringa, Phys. Rev. C **78**, 065501 (2008).

[51] Y.-H. Song *et al.*, Phys. Lett. B **656**, 174 (2007).

[52] E. Adelberger *et al.*, Rev. Mod. Phys. **70**, 1265 (1998).

[53] C. Amsler *et al.* (Particle Data Group), Phys. Lett. B **667**, 1 (2008).

[54] E. Amaldi, S. Fubini, and G. Furlan, Springer Tracts Mod. Phys. **83**, 1 (1979).

[55] T. Kitagaki *et al.*, Phys. Rev. D **28**, 436 (1983).

[56] C. Juszczak, J. T. Sobczyk, and J. Zmuda, Phys. Rev. C **82**, 045502 (2010).

[57] T. R. Hemmert, B. R. Holstein, and N. C. Mukhopadhyay, Phys. Rev. D **51**, 158 (1995).

[58] K. Kubodera, J. Delorme, and M. Rho, Phys. Rev. Lett. **40**, 755 (1978).

[59] I. S. Towner, Nucl. Phys. A **542**, 631 (1992).

[60] M. Kirchbach, D. O. Riska, and K. Tsushima, Nucl. Phys. A **542**, 616 (1992).

[61] M. Chemtob and M. Rho, Nucl. Phys. A **163**, 1 (1971).

[62] J. J. Simpson, Phys. Rev. C **35**, 752 (1987).

[63] Yu. A. Akulov and B. A. Mamyrin, Phys. Lett. B **610**, 45 (2005).

[64] R. Schiavilla, R. B. Wiringa, V. R. Pandharipande, and J. Carlson, Phys. Rev. C **45**, 2628 (1992).

[65] J. Carlson and R. Schiavilla, Rev. Mod. Phys. **70**, 743 (1998).

[66] M. Viviani, R. Schiavilla, and A. Kievsky, Phys. Rev. C **54**, 534 (1996).

[67] R. Lazauskas, Y.-H. Song, and T.-S. Park, arXiv:0905.3119.

[68] T.-S. Park, D.-P. Min, and M. Rho, Phys. Rev. Lett. **74**, 4153 (1995); T.-S. Park, K. Kubodera, D.-P. Min, and M. Rho, Phys. Rev. C **58**, R637 (1998); Phys. Lett. B **472**, 232 (2000).

[69] S. Pastore, L. Girlanda, R. Schiavilla, M. Viviani, and R. B. Wiringa, Phys. Rev. C **80**, 034004 (2009).

[70] S. Kölling, E. Epelbaum, H. Krebs, and U.-G. Meissner, Phys. Rev. C **80**, 045502 (2009).

[71] L. Girlanda, A. Kievsky, L. E. Marcucci, S. Pastore, R. Schiavilla, and M. Viviani, Phys. Rev. Lett. **105**, 232502 (2010).

[72] A. Czarnecki, W. J. Marciano, and A. Sirlin, Phys. Rev. Lett. **99**, 032003 (2007).

[73] S. L. Adler and Y. Dothan, Phys. Rev. **151**, 1267 (1966); N. Kaiser, Phys. Rev. C **67**, 027002 (2003); V. Bernard, N. Kaiser, and U.-G. Meissner, Phys. Rev. D **50**, 6899 (1994).

[74] S. E. Kuhn *et al.*, Phys. Rev. C **50**, 1771 (1994).

[75] R. Bizzarri *et al.*, Nuovo Cimento **33**, 1497 (1964); M. M. Block *et al.*, *ibid.* **55**, 501 (1968).